Chapter 6

A Methodology for Quantum Molecular Modeling of Structure and Reactivity at Solid–Liquid Interfaces

Eugene V. Stefanovich and Thanh N. Truong

Department of Chemistry, University of Utah, Salt Lake City, UT 84112

A QM/MM methodology for modeling chemical reactions at solid-liquid interfaces is presented. This new method combines advances in dielectric continuum solvation models for describing polarization of the liquid with the embedded cluster approach for treating interactions in the solid. In addition, a new method for simple, yet accurate, incorporation of the Madelung potential effect in embedded cluster calculations is discussed. The advantages and accuracy of this method are demonstrated in a number of test calculations. Geometries and adsorption binding energies of H_2O at the NaCl(001)/water interface are calculated and compared with those at the NaCl(001)/vacuum interface.

In recent years the emphasis in quantum chemistry has been shifting from properties of gas-phase molecules and reactions toward challenging areas of condensed phase systems. In particular, molecular processes at solid-liquid interfaces have attracted much attention as they play important roles in environmental chemistry, biochemistry, electrochemistry, heterogeneous catalysis, and other fields. For example, sodium chloride crystals, apart from being a useful model system for theoretical developments, participate in a number of atmospheric processes. Sea salt aerosoles react with various gases, such as NO_2, in the earth's troposphere *(1,2)*. Adsorbed water certainly plays a key role in these reactions. Despite much experimental progress, very little is known for certain regarding mechanisms of interfacial processes. Many experimental surface sensitive techniques such as thermodesorption, scanning tunneling, and photo-electron spectroscopies, require low coverage, ultra-high vacuum, or extreme temperature conditions, thus may be not directly relevant to the solid-liquid interfacial systems found in Nature. Theory can play a crucial role here.

Accurate theoretical modeling of functional groups and sorption complexes at the interface, however, is a difficult task because interfacial energetics are driven by a complicated balance between hydration forces and crystal-solute interactions. Any theory for realistic modeling of chemical reactions at solid-liquid interfaces should provide an accurate description of bond-forming and -breaking processes and interactions of adsorbates and surface defects with the crystal lattice and solvent. Below we discuss some advantages and weaknesses of three common

theoretical approaches that can be employed to study interfacial chemical processes, namely the periodic quantum mechanical, classical molecular mechanics, and quantum embedded cluster methods.

The main advantage of *ab initio periodic supercell* calculations is that they permit an accurate description of interactions between the active surface site and the rest of the crystal. However, periodic models suffer from difficulties with representing the statistical nature of the solvent and cannot avoid spurious interaction between defects or active sites in adjacent unit cells *(3)*. Often these methods are not practical for modeling low-symmetry defect sites and exploring potential energy surfaces. Furthermore, periodic boundary conditions are not particularly suitable for studying charged defects. Full *ab initio* quantum mechanical calculations of solid-liquid interfaces to date are limited to studies of monolayer or bilayer adsorption of water molecules using small surface unit cells *(4-13)* .

Classical *molecular mechanics,* in conjunction with Monte Carlo or molecular dynamics methods, is a powerful tool for analyzing structure and thermodynamic properties of condensed phase systems. In particular, valuable information has been obtained for solvent structure near the MgO-water *(14)* and NaCl-water *(15-17)* interfaces, acidities of hydroxyls at the Fe_2O_3-vacuum interface *(18)*, and stabilization of Al_2O_3 surfaces by hydroxyls *(19)*. However, current molecular force fields do not provide an accurate representation of reactive processes such as dissociative chemisorption. Performance of these approaches depends on advances in development of molecular mechanics force fields which is a difficult and time-consuming task *(20)*.

The quantum *embedded cluster* approach *(21-23)* takes advantage of the localized nature of surface chemical processes, so that only a relatively small molecular system (active center + adsorbate, or *quantum cluster*) can be treated quantum mechanically by accurate *ab initio* or DFT methods using large basis sets. The rest of the crystal lattice and solvent (*environment*) are treated classically. Their action on electrons in the cluster is represented by adding an embedding potential $V_{embed}(\mathbf{r})$ to the quantum Hamiltonian of the cluster. Flexibility and comparatively low computational cost of the embedded cluster approach makes it especially suitable for studies of chemical interactions at solid-liquid interfaces.

In this paper, we discuss applications of our recently proposed quantum cluster methodology, called CECILIA (Combined Embedded Cluster at the Interface with LIquid Approach), for modeling chemical phenomena at non-metal solid-liquid interfaces *(24)*. CECILIA combines advantages of the embedded cluster method discussed above with the dielectric continuum method for solvation. We focus on two important aspects that are critical for the accuracy of the CECILIA model: the solvent polarization field and Madelung potential from the crystalline lattice. These are two long-range components which often make dominant contributions to the total embedding potential $V_{embed}(\mathbf{r})$ for a cluster located at the solid-liquid interface. For solvent polarization, the dielectric continuum approach provides a cost effective methodology and is an active area of research in liquid phase solvation studies (see, for example Generalized COnductor-like Screening MOdel (GCOSMO) calculations in Refs. *(25-31)*), however, its application for solid-liquid interfaces is a new and unexplored area. For ionic and semi-ionic compounds, the Madelung potential from the crystal lattice makes an important contribution to $V_{embed}(\mathbf{r})$. For this contribution we recently proposed a new SCREEP method (Surface Charge Representation of the Electrostatic Embedding Potential; Stefanovich, E.V.; Truong, T.N. *J. Phys. Chem..*, submitted) that can accurately replace the Madelung potential active on a quantum cluster by a potential from a finite set of point charges located on a surface surrounding the cluster. In this chapter we will briefly describe both

GCOSMO and SCREEP methods focusing on their use of a common mathematical technique, i.e., solution of the electrostatic Poisson equation with the boundary condition for an ideal conductor. We also present calculation results for geometries and adsorption binding energies of H_2O at the NaCl(001)/water and NaCl(001)/vacuum interfaces. In the next section we briefly describe the physical model of the solid-liquid interface employed in this study.

A Physical Model of the Solid-Liquid Interface

In our CECILIA approach, the whole system (surface defect + crystal + solvent) is divided into three main regions (Figure 1) designed to maximize the chemical accuracy while keeping the problem tractable by modern computers.

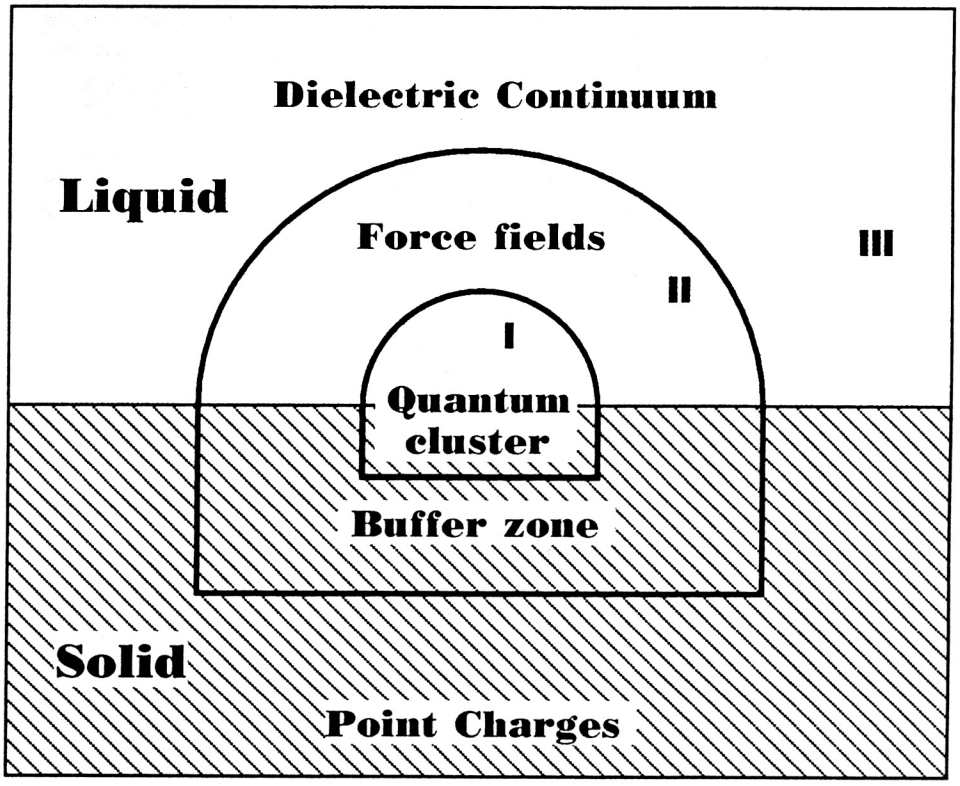

Figure 1. The CECILIA model. (Adapted from Ref. *(24)*)

The innermost quantum mechanical region (I), or *quantum cluster* where chemistry occurs, is treated accurately by either *ab initio* molecular orbital or density functional methods. Normally, the quantum cluster may consist of several lattice atoms near the defect site, the adsorbate, and a few water molecules making strong hydrogen bonds with the surface complex. The *buffer zone* (II) may include several dozen atoms in the crystal lattice and several solvent molecules treated as classical particles surrounding the quantum cluster. This region is designed to describe short-range forces between nuclei and electrons in the quantum cluster and the surrounding medium. The *peripheral zone* (III) provides for a correct Madelung potential from the crystal lattice and the long-range solvent polarization potential in the quantum

cluster and buffer regions. In this paper, we are primarily concerned with an accurate description of the peripheral zone.

In the CECILIA approach, a self-consistent treatment of the solvent polarization is achieved by using the GCOSMO dielectric continuum solvation model in which the liquid is modeled as a dielectric continuum separated from the solute (in our case crystal surface and adsorbate) by a sharp boundary. In homogeneous solvation studies, this boundary is constructed as a set of interlocking spheres centered on nuclei and having fixed radii fitted to experimental hydration free energies of ions and molecules *(31)*. The solvent polarization field is then represented as charge density on the boundary determined self-consistently with the charge density distribution of the solute. We will demonstrate how this methodology can be applied for the solid-liquid interface situation.

To represent the Madelung potential from the crystal lattice acting inside the quantum cluster is not a trivial task even if we assume that the crystal in the peripheral zone is composed of point ions situated at lattice sites. Although in such a case one can easily evaluate the corresponding electrostatic potential $V_{el}(\mathbf{r})$ at any given point in the cluster, for instance by using Ewald summation formulas, the difficulty arises from the necessity to calculate matrix elements $\langle \mu | V_{el}(\mathbf{r}) | \nu \rangle$ over cluster basis functions. One possibility is to perform a direct calculation of matrix elements of the Ewald potential *(32)*. However, implementation of this method (see DICAP *(33)* and EMBED *(34)* codes) requires significant modifications in standard molecular quantum chemistry programs. In addition, no analytical energy derivatives are currently available. A more common methodology is to substitute the infinite lattice by a finite number of point charges placed at ideal lattice sites $\mathbf{R}_j$ that have values corresponding to ionic charges in the crystal *(35-40)*. This method has the advantage that matrix elements of the point-charge potential, as well as their first and second derivatives, are readily available in most quantum chemistry programs (as nuclear attraction integrals). However, construction of such finite lattice models becomes rather difficult for complex low-symmetry crystals. A well-known difficulty for such an approach is that results converge very slowly, if converge at all, when the size of the explicitly considered lattice is increased. Thus, there is no simple way for systematic improvement of results.

To illustrate this poor convergence, consider the electrostatic potential from an infinite 5-layer slab of point charges (±1) parallel to the (001) plane of the rocksalt (NaCl) lattice. Let us first demonstrate the performance of the traditional embedding scheme in which the infinite lattice is substituted by a neutral block with dimensions $n \times n \times m$ (n=6-14, m= 3-5), m layers deep. As an indication of the accuracy we calculated the RMS deviation of the model potential from the exact Ewald potential at 21 equidistant points having z-coordinates between 1.0Å and 5.0Å directly above the surface cation. These results are presented in Table I below. As expected, they show rather poor convergence when the size of the explicitly treated lattice is increased.

Table I. RMS deviations (in kcal/mol) from the exact Madelung potential above the NaCl(001) surface for finite lattice models with dimensions $n \times n \times m$.

$n \times n$	6×6	8×8	10×10	12×12	14×14
m					
3	3.64	1.71	0.97	0.60	0.39
4	2.42	0.83	0.35	0.17	0.09
5	3.10	1.40	0.80	0.51	0.34

In what follows we want to show that accurate representation of both the Madelung potential and the solvent polarization field can be achieved by using basically identical mathematical techniques, i.e., applying the boundary condition for a conductor in the external electrostatic field.

Boundary Condition for a Conductor in the External Electric Field

Consider a region of space C where the charge density is zero and the electrostatic potential is produced by the charge distribution $\rho(\mathbf{r})$ lying entirely outside C. A well-known theorem from electrostatics states that no matter what is the charge distribution $\rho(\mathbf{r})$ *outside* C, its electrostatic potential $V_{el}(\mathbf{r})$ *inside* C can be rigorously replaced by some surface charge density $\sigma(\mathbf{r})$ located on the *boundary* S of the volume C. The demonstration goes as follows. First assume that we have filled the volume C (interior of the surface S) with an ideal metallic conductor. The electrostatic potential inside S becomes exactly zero independent of the external potential $V_{el}(\mathbf{r})$. Physically, this condition is satisfied due to creation of the charge density $-\sigma(\mathbf{r})$ on the surface S whose potential $-\oint_S \frac{\sigma(\mathbf{r}')}{|\mathbf{r}-\mathbf{r}'|} d^2r$ exactly compensates the external potential $V_{el}(\mathbf{r})$ for all points $\mathbf{r}$ on the surface S and in its interior.

$$V_{el}(\mathbf{r}) - \oint_S \frac{\sigma(\mathbf{r}')}{|\mathbf{r}-\mathbf{r}'|} d^2r = 0 \qquad (1)$$

This means that the electrostatic potential generated by the charge density $\sigma(\mathbf{r})$ on the surface S and in its interior is exactly equal to the original potential $V_{el}(\mathbf{r})$. (The potential generated by $\sigma(\mathbf{r})$ *outside* the surface S is generally different from $V_{el}(\mathbf{r})$).

For computational reasons, we resort to the boundary element method to represent the continuous surface charge density $\sigma(\mathbf{r})$ on the surface S by a set of M point charges q_j located at the centers $\mathbf{r}_j$ of surface elements with areas S_j.

$$q_j \approx \sigma(\mathbf{r}_j) S_j \qquad (2)$$

This approximation is accurate when the number of surface points M is large enough, and the charge distribution $\sigma(\mathbf{r})$ is sufficiently smooth. Then Eq. (1) can be approximated by a matrix equation

$$V - \mathbf{A}\mathbf{q} = 0 \qquad (3)$$

from which the vector of surface charges $\mathbf{q}$ can be determined by applying any common technique available for solving systems of linear equations. For example, one can use the matrix inversion method.

$$\mathbf{q} = \mathbf{A}^{-1} V \tag{4}$$

In Eqs. (3) and (4), the vector V contains values of the external electrostatic potential at points $\mathbf{r}_j$ ($V_j = V_{el}(\mathbf{r}_j)$), and **A** is the $M \times M$ non-singular matrix with matrix elements.

$$A_{ij} = \frac{1}{|\mathbf{r}_j - \mathbf{r}_i|} \quad \text{for } j \neq i, \text{ and } A_{jj} = 1.07\sqrt{\frac{4\pi}{S_j}} \tag{5}$$

Non-diagonal elements A_{ij} represent a generic Coulomb interaction between surface elements $\mathbf{r}_i$ and $\mathbf{r}_j$. The diagonal elements A_{jj} describe the self-interaction of the surface element $\mathbf{r}_j$. This self-interaction was discussed in detail by Klamt and Shüürmann *(41)*, and the coefficient 1.07 was fitted by these authors for better numerical accuracy.

The CECILIA Model

The computational method described above was first applied by Klamt and Shüürmann *(41)* in their COSMO (COnductor-like Screening MOdel) dielectric continuum model for solvation in the bulk liquid. The virtue of using conductor boundary conditions for aqueous solvent comes from the fact that water has a rather high dielectric constant (ε =78.3), thus screening properties of the solvent are similar to those of an ideal conductor. Therefore, in the first approximation of the CECILIA model, liquid can be represented as a conductor in the electrostatic field generated by the crystal and adsorbate. Two points should be made. First, one should correct conductor surface charges to account for the finite dielectric constant of water. Second, surface charges should be determined self-consistently with the electronic and atomic structure of the quantum cluster. Thus, instead of Eq. (4), the equation for surface charges is

$$\mathbf{q} = -\frac{\varepsilon - 1}{\varepsilon}\mathbf{A}^{-1} V \tag{6}$$

where the vector V contains electrostatic potentials produced by the charge density of the crystal at points $\mathbf{r}_j$ on the dielectric cavity. This potential can be conveniently separated into contributions from classical particles (atomic nuclei in the quantum cluster and classical particles in the buffer and peripheral zones) with charges z_i and positions $\mathbf{R}_i$ and from the electron density $\rho(\mathbf{r})$ in the quantum cluster

$$V_j = V_j^{class} + V_j^{el} = \sum_i \frac{z_i}{|\mathbf{r}_j - \mathbf{R}_i|} - \int \frac{\rho(\mathbf{r})}{|\mathbf{r} - \mathbf{r}_j|} d^3 r \tag{7}$$

Correspondingly, surface charges in Eq. (6) can be separated into "classical" $\mathbf{q}^{class}$ and "electronic" $\mathbf{q}^{el}$ components. The classical surface charges are taken into account by adding the term

$$H^{s}_{\mu\nu} = \mathbf{q}^{class}\mathbf{L}_{\mu\nu} + W^{buf}_{\mu\nu} + \langle\mu|V_{el}(\mathbf{r})|\nu\rangle \tag{8}$$

to the one-electron part of the Fock matrix for an isolated cluster ($H^{0}_{\mu\nu}$). Here $L^{j}_{\mu\nu}$ are matrix elements of the potential generated by a unit point charge at the point $\mathbf{r}_j$ on the dielectric cavity. In contrast to the GCOSMO Hamiltonian for a solute in the bulk liquid *(30)*, this expression contains additional matrix elements of the short-range embedding potential $W^{buf}_{\mu\nu}$ from the buffer zone and Madelung potential $\langle\mu|V_{el}(\mathbf{r})|\nu\rangle$ from the buffer and peripheral zones. The former term may be represented by different embedding techniques including the pseudoatom *(42)*, localized orbitals *(43)*, density functional *(44)*, or pseudopotential *(33,45-48)* methods. For such ionic compound as NaCl, the pseudopotential form of $W^{buf}_{\mu\nu}$ has been found to be rather accurate. The Madelung potential term will be discussed in more detail in the next Section. Another difference with the bulk solvation case is that the surface of the cavity is not closed. Only the quantum cluster and its nearest neighbors on the crystal surface need to be solvated to obtain relative energies of surface configurations *(24)*. The contribution of electronic surface charges $\mathbf{q}^{el}$ to the two-electron part of the Fock matrix is given by

$$G^{s}_{\mu\nu} = \mathbf{q}^{el}\mathbf{L}_{\mu\nu} \tag{9}$$

Then, the self-consistency between the electron density and solvent polarization field is achieved in a single SCF procedure by calculating $\mathbf{q}$ and $G^{s}_{\mu\nu}$ from Eqs. (6) and (9), respectively, at each iteration.

The total energy of the quantum cluster at the solid-liquid interface in HF and DFT methods is expressed as

$$\begin{aligned} E_{tot} = & \sum_{\mu\nu}\left[P_{\mu\nu}\left(H^{0}_{\mu\nu}+H^{s}_{\mu\nu}\right)+\tfrac{1}{2}P_{\mu\nu}\left(G^{0}_{\mu\nu}+G^{s}_{\mu\nu}\right)\right] \\ & +\mathbf{q}^{class}V^{class} + E_{nn} + E_{non-els} \end{aligned} \tag{10}$$

where $P_{\mu\nu}$ is the converged density matrix of the quantum cluster, E_{nn} is the energy of interaction between classical particles, i.e. nuclei in the QM cluster and ions in the buffer and point charge zones. Apart from Coulomb interactions, this term may include short-range potentials taken from various force-fields. $E_{non-els}$ contains non-electrostatic dispersion-repulsion and cavity formation contributions to the solvation free energy. First and second derivatives of the total energy (6) with respect to the coordinates of atoms in the cluster and buffer zone are available *(25)*. This allows for efficient geometry optimization of adsorbate structures at solid-liquid interfaces.

The SCREEP Model

The conductor boundary conditions discussed above can also be used to conveniently replace the Madelung potential in the quantum cluster by a finite set of point charges. This allows for straightforward calculation of corresponding matrix elements $\langle \mu | V_{el}(\mathbf{r}) | \nu \rangle$. Let us first define a closed surface S such that all quantum cluster atoms and the GCOSMO dielectric cavity lie inside this surface (see Figure 2).

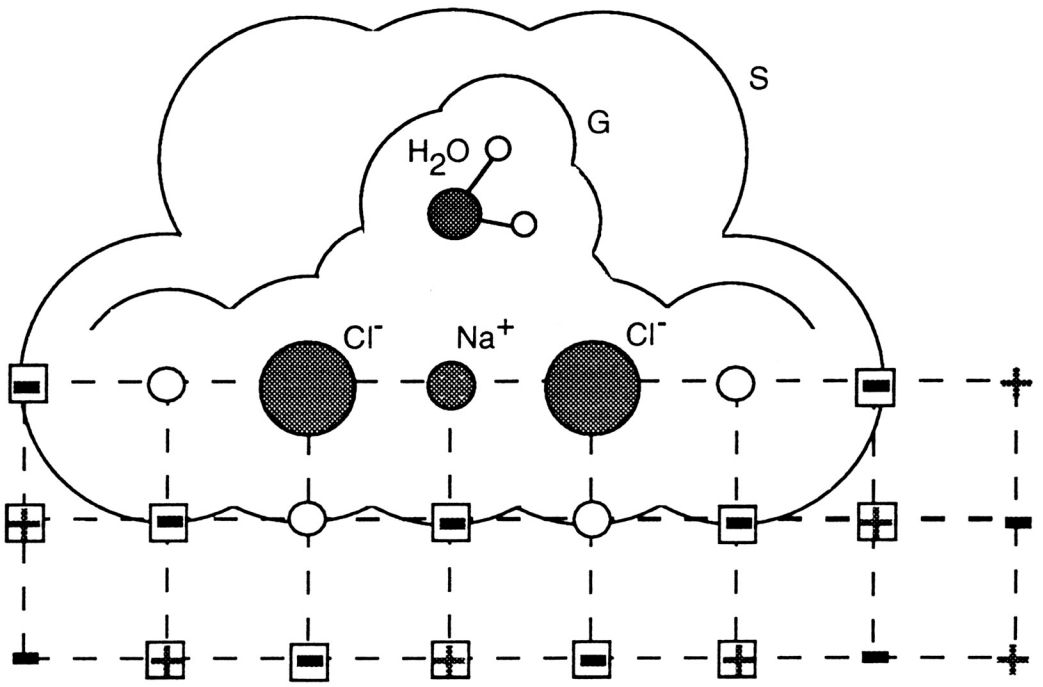

Figure 2. Side view of the $[Na_5Cl_4+H_2O]^+$ cluster on the NaCl(001) surface and sketch of the CECILIA model. Shaded circles are ions from the quantum cluster; empty circles are Na^+ ECPs from the buffer zone; "+" and "-" symbols inside squares denote point charges in the explicit zone; the potential from other lattice charges is modeled by the charge density on the SCREEP surface S; surface G is the dielectric continuum cavity.

As in continuum solvation methods, surface S can be constructed as a set of interlocking spheres of radius R_a centered on cluster nuclei and discretized into a finite number of surface elements. Then Madelung potentials on the surface elements can be calculated by using the Ewald summation technique (note that the contribution from lattice ions inside the surface S should be subtracted from the Ewald sum) and values of surface charges $\mathbf{q}$ can be obtained from Eq. (4). The potential generated by these charges can be used as a substitute for the Madelung potential inside the surface S, i.e., in the quantum cluster and on the GCOSMO dielectric cavity.

Our analysis of the SCREEP approximation revealed two important points. First, the radius R_a should be large enough so that a major part of the cluster wave function is contained inside the surface S. Second, for better accuracy of the

SCREEP model one should treat explicitly the potential from lattice ions lying close to the quantum cluster. This means that we directly include the potential of these ions in calculation of $\langle \mu | V_{el}(\mathbf{r}) | \nu \rangle$ and subtract this potential from the vector V used in Eq. (4). Moreover, the explicit zone (shown schematically by "+" and "-" symbols inside squares in Figure 2) should be selected in such a way that its total charge is zero or small.

Calculation Details

In the rest of this paper we consider applications of the SCREEP and CECILIA methods to study water molecule adsorption on the unrelaxed rock-salt NaCl(001) surface and NaCl(001)-water interface. The quantum cluster $[Na_5Cl_4+H_2O]^+$ selected for these studies contained nine surface atoms that form a square 3×3 substrate and adsorbed water molecule (Figure 2). As NaCl is a rather ionic crystal, we do not expect that slight deviation from stoichiometry and assignment of the integer charge (+1) to this cluster will affect results in any significant way. Geometries for water molecules in different environments (gas phase, liquid phase, adsorbed on the clean surface, and adsorbed at the interface) were fully optimized at the pseudopotential Hartree-Fock level. The oxygen atom was described by the SBK effective core pseudopotentials (ECP) and CEP-31+G* basis set *(49)*. The 311++G** basis set was used for hydrogens. Na and Cl ions were described by the Hay-Wadt ECP and standard valence double-zeta basis sets *(50)*. Electron correlation was included at the MP2 level as single point calculations at HF optimized geometries. Dissociation and adsorption energies were calculated as total energy differences between the compound system and its separated fragments.

The short-range embedding potential $W_{\mu\nu}^{buf}$ (exchange, Pauli repulsion) was represented by Hay-Wadt ECP for Na^+ cations that are nearest neighbors to the quantum cluster. More distant Na^+ ions can be rather accurately treated as point charges (q=+1). Actually, when they were treated as pseudopotentials, cluster energies changed by less than 0.1 kcal/mol. We are not aware of any accurate whole-ion pseudopotential representation of lattice Cl^-. However, as indicated in Refs. *(33,45)*, the ground-state electron density in the quantum cluster only slightly penetrates surrounding anions, therefore they can be described rather accurately in the point charge (q=-1) approximation.

Cavities for SCREEP and CECILIA calculations were constructed using the gepol93 algorithm *(51)* as a set of interlocking spheres centered on atoms. The dielectric cavity adjusted automatically when atoms in the quantum region moved during the geometry optimization, while the SCREEP surface remained fixed. Each complete atomic sphere contained 60 surface charges. Atomic radii for the CECILIA cavity were taken from our previous work *(24,31)*: 1.172 Å for H, 1.576 Å for O, 1.61 Å for Na, and 1.75 Å for Cl. The cavity boundary was truncated so that only atoms in the cluster and their nearest neighbors on the surface were solvated. The effect of suc'. truncation was found to be insignificant. For example, when the boundary was truncated so that only cluster atoms were solvated, the adsorption energies changed by less than 0.1 kcal/mol.

The SCREEP surface S was constructed by making spheres of radius R_a= 2.5 Å around each atom in the cluster and around 9 additional centers having z-coordinates of 4.0 Å just above each atom in the cluster (Figure 2). Introduction of these additional centers comes from the necessity to provide enough space for placing adsorbate molecules inside the SCREEP surface above the crystal. Using the same accuracy criterion as in Table I, we found that the SCREEP method gives a

much more accurate (RMS error of less than 0.01 kcal/mol) Madelung potential than any finite lattice $n \times n \times m$ representation shown in Table I.

The term $E_{non-els}$ in eq. (10) was calculated using methods described in Refs. *(52,53)* with the optimized solvent water radius of 1.29 Å *(31)*. We used the OPLS force field parameters *(54)* for calculating dispersion-repulsion interactions with the solvent in this work. All calculations were performed by using our locally modified version of the Gaussian92/DFT computer code *(55)*.

Results and Discussion

Let us first compare three embedding schemes for H_2O adsorption on the NaCl(001)-vacuum interface: no embedding at all, i.e., adsorption on the bare $[Na_5Cl_4]^+$ cluster; embedding in the finite $8 \times 8 \times 4$ lattice of point charges (±1) (247 explicit lattice ions outside cluster); and the SCREEP embedding scheme (121 lattice ions in the explicit zone plus 422 point charges on the surface S). These results are presented in the first three columns in Table II.

Table II. Geometry (distances in Å, angles in degrees)[a] and adsorption energy (kcal/mol) for H_2O molecule adsorbed on the NaCl(001) surface calculated using the $[Na_5Cl_4+H_2O]^+$ quantum cluster and different embedding schemes. The most accurate results are shown in bold.

	Solid-vacuum interface				*Solid-liquid interface*	
Madelung potential	no	8×8×4	SCREEP	8×8×4	8×8×4	SCREEP
Buffer zone	no	no	no	ECP	ECP	ECP
Solvent effects	no	no	no	no	yes	yes
Oz	2.390 [2.43][c]	2.384	2.380	**2.401**	2.599	**2.597**
Ox=Oy	0.294	0.374	0.375	**0.409**	0.057	**0.047**
OH	0.948	0.949	0.949	**0.949**	0.952	**0.952**
HOH angle	106.4	106.2	106.2	**98.3**	104.5	**104.4**
tilt angle	19.6 [30.5][c]	5.4	5.9	**0.3**	11.9	**12.8**
Adsorption energy	7.5 [7.8][c]	8.3	8.3	6.7 (**8.1**)[b]	3.6 (5.5)[b]	3.6 (**5.5**)[b]

[a] The origin was placed at the central Na^+ ion in the cluster; x and y axes were directed toward nearest surface Cl^- ions; the z-axis pointed outside the crystal.

[b] In parentheses results of MP2 single-point calculations.

[c] In square brackets theoretical results from Ref. *(56)*.

H_2O adsorbs on the NaCl(001) surface with oxygen above the Na^+ site and hydrogen atoms pointing symmetrically toward nearest anions and slightly away from the surface *(24)*. As seen from Table II, the neglect of the Madelung field in the cluster leads to some increase of the oxygen-surface distance and molecular tilt angle (the angle between the molecular axis and the surface). This comparison may explain why recent *ab initio* calculations of H_2O/NaCl(001) adsorption using the Na_9Cl_9 cluster without any embedding potential *(56)* overestimate these parameters. The adsorption energy calculated by these authors (7.8 kcal/mol) is

also close to our result for the bare cluster (7.5 kcal/mol). Results for $8 \times 8 \times 4$ and SCREEP embedding schemes agree with each other but differ significantly from those for the bare cluster. Comparison of the $8 \times 8 \times 4$ and SCREEP embedding schemes serves two purposes. First, it confirms our correct implementation of the SCREEP method. Second, it indicates that traditional finite lattice embedding (the $8 \times 8 \times 4$ lattice in our case) may be quite successful for simple crystal lattices if proper care is taken in selecting the finite lattice size *(24,44,57,58)*. Thus, real benefits of using SCREEP embedding can be revealed in studies of complex crystal lattices, such as zeolites, where traditional embedding models are not easy to construct.

The importance of the non-electrostatic short-range embedding potential ($W_{\mu\nu}^{buf}$ in eq. (8)) can be seen by comparing results from the second column in Table II with calculations in which cations nearest to the quantum cluster were represented by Na^+ effective core pseudopotentials (4th column in Table II). The latter more accurate treatment leads to a decrease of the adsorption energy by 1.6 kcal/mol, decrease of the molecular tilt angle by 5.1 degree and increase of the adsorption distance by 0.017 Å. Taking into account correlation effects at the MP2 level, the adsorption energy of 8.1 kcal/mol is in reasonable agreement with experimental data (8.5-13.1 kcal/mol, see Ref. *(24)*). Note that the adsorption energy is likely to be overestimated in experiments due to the presence of surface defects.

Results for H_2O adsorption at the NaCl-water interface are shown in the 5th ($8 \times 8 \times 4$ embedding) and 6th (SCREEP embedding) columns in Table II. In both cases, Na^+ pseudopotentials were used in the buffer zone. As expected, both embedding models give similar results. The screening effect of the solvent reduces attraction of the H_2O molecule to surface ions (compare with results in the 4th column). The distance of the oxygen atom from the surface increases by 0.2 Å. H atoms no longer feel a strong attraction to Cl^- lattice anions, therefore, the tilt angle between the molecular axis and surface plane increases from 0.3 to 12-13 degrees, the lateral shift of the molecule along the <110> axis decreases substantially, and the HOH angle increases to the value of 104.4 characteristic for the hydrated water molecule. In general, the internal structure of the H_2O molecule adsorbed at the interface is much closer to the geometry of hydrated H_2O than to the geometry of water adsorbed at the clean NaCl(001) surface. In agreement with these results, dielectric screening by the solvent reduces the interaction energy between H_2O and the solid surface by about 2.6 kcal/mol. However, there is still a noticeable attraction (5.5 kcal/mol) which immobilizes the H_2O molecule near the NaCl surface in agreement with previous molecular dynamics simulations*(15,17)* and a helium atom scattering study *(16)*. About half of this adsorption energy (2.6 kcal/mol) is due to non-electrostatic solvation effects *(24)*.

Conclusion

We presented a general methodology for *ab initio* embedded cluster calculations of reactivity at the solid-liquid interface (CECILIA model). A new important component of this model is the SCREEP method which allows to accurately represent the Madelung potential in embedded cluster calculations of solids. With appropriate choice of computational parameters, the SCREEP method can easily provide a RMS deviation of less than 0.1 kcal/mol from the exact lattice potential. It is important that this method requires only a negligible increase (1-2%) of the computational time in our quantum embedded cluster calculations as compared to the bare molecule calculation, and the accuracy level can be improved in a simple and systematic way. Moreover, no modifications to existing molecular quantum

chemistry programs were required. Positions and values of surface charges need to be determined only once from a separate simple calculation. In addition to efficient geometry optimization, our current implementation of the CECILIA and SCREEP approaches allows for calculation of vibrational frequencies and excited states. Extensive studies of adsorption and reactions at MgO-water, TiO_2-water, and Al_2O_3-water interfaces are currently underway in our laboratory.

Acknowledgment

This work was supported in part by the National Science Foundation through a Young Investigator Award to T.N.T.

Literature Cited

(1) Vogt, R.; Finlayson-Pitts, B. J. *J. Phys. Chem.* **1995**, *99*, pp 17269-17272.
(2) Langer, S.; Pemberton, R. S.; Finlayson-Pitts, B. J. *J. Phys. Chem. A* **1997**, *101*, pp 1277-1286.
(3) Anchell, J. L.; Hess, A. C. *J. Phys. Chem.* **1996**, *100*, pp 18317-18321.
(4) Goniakowski, J.; Gillan, M. J. *Surf. Sci.* **1996**, *350*, pp 145-158.
(5) Lindan, P. J. D.; Harrison, N. M.; Holender, J. M.; Gillan, M. J. *Chem. Phys. Lett.* **1996**, *261*, pp 246-252.
(6) Fahmi, A.; Minot, C. *Surf. Sci.* **1994**, *304*, pp 343-359.
(7) Podloucky, R.; Steinemann, S. G.; Freeman, A. J. *New J. Chem.* **1992**, *16*, pp 1139-1143.
(8) Scamehorn, C. A.; Hess, A. C.; McCarthy, M. I. *J. Chem. Phys.* **1993**, *99*, pp 2786-2795.
(9) Scamehorn, C. A.; Harrison, N. M.; McCarthy, M. I. *J. Chem. Phys.* **1994**, *101*, pp 1547-1554.
(10) Taylor, D. P.; Hess, W. P.; McCarthy, M. I. *J. Phys. Chem. B* **1997**, *101*, pp 7455-7463.
(11) Orlando, R.; Pisani, C.; Ruiz, E.; Sautet, P. *Surf. Sci.* **1992**, *275*, pp 482-492.
(12) Ursenbach, C. P.; Voth, G. A. *J. Chem. Phys.* **1995**, *103*, pp 7569-7575.
(13) Langel, W.; Parrinello, M. *J. Chem. Phys.* **1995**, *103*, pp 3240-3252.
(14) McCarthy, M. I.; Schenter, G. K.; Scamehorn, C. A.; Nicholas, J. B. *J. Phys. Chem.* **1996**, *100*, pp 16989-16995.
(15) Anastasiou, N.; Fincham, D.; Singer, K. *J. Chem. Soc. Faraday Trans. II* **1983**, *79*, pp 1639-1651.
(16) Bruch, L. W.; Glebov, A.; Toennies, J. P.; Weiss, H. *J. Chem. Phys.* **1995**, *103*, pp 5109-5120.
(17) Wassermann, B.; Mirbt, S.; Reif, J.; Zink, J. C.; Matthias, E. *J. Chem. Phys.* **1993**, *98*, pp 10049-10060.
(18) Rustad, J. R.; Felmy, A. R.; Hay, B. P. *Geochim. Cosmochim. Acta* **1996**, *60*, pp 1563-1576.
(19) Nygren, M. A.; Gay, D. H.; Catlow, C. R. A. *Surf. Sci.* **1997**, *380*, pp 113-123.
(20) Chacon-Taylor, M. R.; McCarthy, M. I. *J. Phys. Chem.* **1996**, *100*, pp 7610-7616.
(21) *Electronic properties of solids using cluster methods*; Kaplan, T. A.; Mahanti, S. D., Eds.; Plenum: New York, 1995.
(22) Pacchioni, G.; Bagus, P. S. In *Cluster Models for Surface and Bulk Phenomena*; G. Pacchioni, Ed.; Plenum Press: New York, 1992.
(23) *Quantum mechanical cluster calculations in solid state studies*; Grimes, R. W.; Catlow, C. R. A.; Shluger, A. L., Eds.; World Scientific: Singapore, 1992.
(24) Stefanovich, E. V.; Truong, T. N. *J. Chem. Phys.* **1997**, *106*, pp 7700-7705.
(25) Stefanovich, E. V.; Truong, T. N. *J. Chem. Phys.* **1996**, *105*, pp 2961-2971.

(26) Truong, T. N.; Stefanovich, E. V. *J. Phys. Chem.* **1995**, *99*, pp 14700-14706.
(27) Truong, T. N.; Stefanovich, E. V. *J. Chem. Phys.* **1995**, *109*, pp 3709-3716.
(28) Truong, T. N.; Nguyen, U. N.; Stefanovich, E. V. *Int. J. Quant. Chem.: Quant. Chem. Symp.* **1996**, *30*, pp 403-410.
(29) Truong, T. N.; Truong, T.-T. T.; Stefanovich, E. V. *J. Chem. Phys.* **1997**, *107*, pp 1881-1889.
(30) Truong, T. N.; Stefanovich, E. V. *Chem. Phys. Lett.* **1995**, *240*, pp 253-260.
(31) Stefanovich, E. V.; Truong, T. N. *Chem. Phys. Lett.* **1995**, *244*, pp 65-74.
(32) Saunders, V. R.; Freyria-Fava, C.; Dovesi, R.; Salasco, L.; Roetti, C. *Mol. Phys.* **1992**, *77*, pp 629-665.
(33) Puchin, V. E.; Shluger, A. L.; Tanimura, K.; Itoh, N. *Phys. Rev. B* **1993**, *47*, pp 6226-6240.
(34) Pisani, C.; Orlando, R.; Nada, R. In *Cluster Models for Surface and Bulk Phenomena*; G. Pacchioni; P. S. Bagus and F. Parmigiani, Ed.; Plenum: New York, 1992; pp 515-531.
(35) Harding, H. H.; Harker, A. H.; Keegstra, P. B.; Pandey, R.; Vail, J. M.; Woodward, C. *Physica B & C* **1985**, *131*, pp 151-156.
(36) Allouche, A. *J. Phys. Chem.* **1996**, *100*, pp 1820-1826.
(37) Allouche, A. *J. Phys. Chem.* **1996**, *100*, pp 17915-17992.
(38) Ferrari, A. M.; Pacchioni, G. *J. Phys. Chem.* **1996**, *100*, pp 9032-9037.
(39) Ferro, Y.; Allouche, A.; Corà, F.; Pisani, C.; Girardet, C. *Surf. Sci.* **1995**, *325*, pp 139-150.
(40) Pacchioni, G.; Ferrari, A. M.; Márquez, A. M.; Illas, F. *J. Comp. Chem.* **1997**, *18*, pp 617-628.
(41) Klamt, A.; Schüürmann, G. *J. Chem. Soc., Perkin Trans. II* **1993**, pp 799.
(42) Sauer, J. *Chem. Rev.* **1989**, *89*, pp 199-255.
(43) Gorb, L. G.; Rivail, J.-L.; Thery, V.; Rinaldi, D. *Int. J. Quant. Chem.: Quant. Chem. Symp.* **1996**, *30*, pp 1525-1536.
(44) Stefanovich, E. V.; Truong, T. N. *J. Chem. Phys.* **1996**, *104*, pp 2946-2955.
(45) Winter, N. W.; Pitzer, R. M.; Temple, D. K. *J. Chem. Phys.* **1987**, *87*, pp 2945-2953.
(46) Kunz, A. B.; Vail, J. M. *Phys. Rev. B* **1988**, *38*, pp 1058-1063.
(47) Kunz, A. B.; Klein, D. L. *Phys. Rev. B* **1978**, *17*, pp 4614-4619.
(48) Shidlovskaya, E. K. *Latvian J. Phys. Techn. Sci.* **1996**, *4*, pp 57-82.
(49) Stevens, W.; Basch, H.; Krauss, J. *J. Chem. Phys.* **1984**, *81*, pp 6026-6033.
(50) Wadt, W. R.; Hay, P. J. *J. Chem. Phys.* **1985**, *82*, pp 284-298.
(51) Pascual-Ahuir, J. L.; Silla, E.; Tuñon, I. *J. Comp. Chem.* **1994**, *15*, pp 1127-1138.
(52) Floris, F. M.; Tomasi, J.; Pascual-Ahuir, J. L. *J. Comp. Chem.* **1991**, *12*, pp 784-791.
(53) Pierotti, R. A. *J. Phys. Chem.* **1963**, *67*, pp 1840-1845.
(54) Jorgensen, W. L.; Tirado-Rives, J. *J. Am. Chem. Soc.* **1988**, *110*, pp 1657-1666.
(55) *GAUSSIAN 92/DFT*; Frisch, M. J.; Trucks, G. W.; Schlegel, H. B.; Gill, P. M. W.; Johnson, B. G.; Wong, M. W.; Foresman, J. B.; Robb, M. A.; Head-Gordon, M.; Replogle, E. S.; Gomperts, R.; Andres, J. L.; Raghavachari, K.; Binkley, J. S.; Gonzalez, C.; Martin, R. L.; Fox, D. J.; Defrees, D. J.; Baker, J.; Stewart, J. J. P.; Pople, J. A., Gaussian, Inc.: Pittsburgh, PA, 1993.
(56) Jug, K.; Geudtner, G. *Surf. Sci.* **1997**, *371*, pp 95-99.
(57) Stefanovich, E. V.; Truong, T. N. *J. Chem. Phys.* **1995**, *102*, pp 5071-5076.
(58) Johnson, M. A.; Stefanovich, E. V.; Truong, T. N. *J. Phys. Chem. B* **1997**, *101*, pp 3196-3201.